On-line model-based fault detection and isolation for PEM fuel cell stack systems

A. Rosich[a], R. Sarrate[b], F. Nejjari[b]

[a] *Interdisciplinary Centre for Security Reliability and Trust (SnT), University of Luxembourg, 4 rue Alphonse Weicker, L-2721 Luxembourg*
[b] *Automatic Control Department, Universitat Politècnica de Catalunya (UPC), Rambla Sant Nebridi 10, 08222 Terrassa, Spain*

Abstract

Efficient and reliable operation of Polymer Electrolyte Membrane (PEM) fuel cells are key requirements for their successful commercialization and application. The use of diagnostic techniques enables the achievement of these requirements. This paper focuses on model-based Fault Detection and Isolation (FDI) for PEM fuel cell stack systems. The work consists in designing and selecting a subset of consistency relations such that a set of predefined faults can be detected and isolated. Despite a nonlinear model of the PEM fuel cell stack system will be used, consistency relations that are easily implemented by a variable back substitution method will be selected. The paper also shows the significance of structural models to solve diagnosis issues in complex systems.

Keywords: Fault diagnosis, Consistency relation, Residual generation, Fuel cell system

1. Introduction

Polymer Electrolyte Membrane (PEM) fuel cells are ones of the most promising technologies to be used, in a near future, as power supply sources in many portable applications (e.g. automobiles, aerospace, remote stations, etc.). For this reason, maintenance operations cannot always be properly performed or are expensive to carry out. Thus, the task of monitoring the correct operation of this systems is crucial. In order to perform such a task, efficient diagnosis systems to detect and isolate incipient faults in the PEM fuel cell system must be developed.

In the literature, the works devoted to diagnosis for Fuel Cell Stack (FCS) systems can be roughly divided in two groups. On one hand, there are works designing ad-hoc techniques that use a specialised and specific knowledge to perform diagnosis on the cell stack. Some examples of such techniques are the *polarisation curve*, the *current interruption* or the *electrochemical impedance spectroscopy* methods [1] [2]. Such techniques have demonstrated to have good results for detecting malfunctions inside the cell stack (e.g. fuel cell membrane flooding or/and drying). On the other hand, there are other fault diagnosis techniques based on models. For instance, in [3] faults are diagnosed in an FCS system by using Bayesian networks. In [4], a set of tests are designed from a linear FCS model. Test quantities design techniques are also used in [5], where two tests are developed to detect hydrogen leaks in the anode side. Finally, in [6], a set of structured residuals is obtained from a bond-graph model of a FCS system. The advantage of working with model-based methods is that they are model dependent and thus more robust to modifications of the system. This permits to apply the same method (some-

times with a slight modification) to different system configurations as long as its corresponding model is provided. This is the main reason why model-based diagnosis methods are usually chosen to diagnose faults in the whole FCS system rather than ad-hoc methods valid only for a specific system.

Considerable research has been done in developing such model-based diagnosis systems [7]. Traditionally, diagnosis systems have been developed for linear systems by first linearizing the model and then applying robust techniques to the residual generator design [8]. However, a model linearization approach is not feasible for FCS systems due to the complexity of such systems, that involve a wide range of non-linear equations (lookup tables, polynomial functions, saturations, non-linear dynamic equations, etc.), and moreover their operating point changes. Nevertheless, a non-linear model thoroughly describes the non faulty behavior for different operating points. Therefore, in this present work, non-linear equations are directly applied in the fault diagnosis system design. Despite the nonlinear nature of the model, only residuals that are easily implemented by a variable back substitution method will be selected for the diagnosis system.

In this paper, a complete FCS system model developed in [9] is used to derive the diagnosis system. Based on this FCS model, a set of faults to be detected and isolated is defined. The aim of the work is to use the structural information contained in the model and to design a subset of consistency relations to detect and isolate the set of predefined faults in an FCS system. Then, a set of residuals that can be easily implemented by a simple back substitution method are generated and tested for fault diagnosis.

In Section 2, a review of model-based fault diagnosis is given. In Section 3,

the FCS system is described and a set of faults is defined. In Section 4, a set of consistency relations is designed based on the FCS system model. Simulation results are given in Section 5, and the main conclusions are presented in Section 6.

2. Model-based diagnosis review

2.1. Consistency relations

Model-based fault diagnosis is a consolidated research area, with many published works, within the control field [7], [8]. Most approaches to detect and isolate faults are based on consistency checking. The basic idea behind all these works is the comparison between the observed behavior of the process and its corresponding model. This is performed by means of *consistency relations*. A consistency relation can be roughly described as a function of the form:

$$h(\mathbf{y}(t), \mathbf{u}(t)) = 0 \tag{1}$$

where $\mathbf{y}(t)$ and $\mathbf{u}(t)$ are vectors of known variables, denoting respectively process measurements and process control inputs. Function h is obtained from the model and is the basis to generate a residual:

$$r(t) = h(\mathbf{y}(t), \mathbf{u}(t)) \tag{2}$$

A residual is a temporal signal indicating how close is behaving the process compared with its expected behavior predicted by the model. At the absence of faults, the residual equals zero. In fact, a threshold based test is usually implemented in order to cope with noise and model uncertainty

effects. Otherwise, when a fault is present the model is no longer consistent with the observations (known process variables) and the residual diverges from zero.

Detecting faults is possible with only one residual sensitive to all faults. However, fault isolation is usually required rather than just detecting the presence of a fault. The fault isolation task is performed by designing a set of residuals from different consistency relations. Each residual is sensitive to different faults such that the residual fault signature is unique for each fault. Therefore, distinguishing the actual fault from other faults is possible by looking at the residual fault signature.

A key point in model-based diagnosis relies on the design of consistency relations. For static or dynamic linear models, computing the required consistency relations can be straightforwardly done by means of linear transformations. Nevertheless, consistency relations design becomes trickier for non-linear models.

2.2. Structural model-based diagnosis

One widely accepted approach to handle non-linear models is to represent them by a graph [7]. More formally, given a model composed of equations which depend on a set of unknown variables X and a set of known variables Z (i.e. measured and controlled variables in vectors $\mathbf{y}$ and $\mathbf{u}$, respectively), the corresponding *structural model* is a bipartite graph, $G = (M, V; A)$, where M is the set of equation vertices, $V = X \cup Z$ is the set of variable vertices and A is the set of edges such that

$$A = \{(m, v) \mid \text{variable } v \in V \text{ appears in equation } m \in M\} \tag{3}$$

Alternatively, a structural model is described by a biadjacency matrix which relates equations (rows) and variables (columns). Then, the set of edges of the corresponding bipartite graph is represented by a set of crosses in the biadjacency matrix.

Generating a consistency relation from a structural model entails finding a subset of equations, $M' \subseteq M$, that depend on a subset of unknown variables $X' \subseteq X$ such that there exists a complete matching of X' into M' and

$$|M'| = |X'| + 1 \tag{4}$$

where $|\cdot|$ denotes the cardinality of the set. A matching of a bipartite graph is a subset of edges such that no two edges share a common vertex. A complete matching of X' into M' means that all variables in X' are covered by the matching. Theoretically speaking, the variables in $|X'|$ can be computed from $|M'| - 1$ equations in M', and then the remaining equation is used to derive the consistency relation. Since all unknown variables have been computed, the remaining equation will be in the form of Equation (1). There exist in the literature several algorithms to compute all M' subsets given a structural model [10] [11].

However, designing a consistency relation is not always possible since it requires a feasible computation of all unknown variables. In [12], a framework that takes into account the causal computability concept is described. In order to ensure the computability of every unknown variable, the set of edges is divided into two disjoint subsets:

- $A_{\times} = \{(m, x) \in A \mid x \in X \text{ is causally computable in } m\}$
- $A_{\Delta} = \{(m, x) \in A \mid x \in X \text{ is not causally computable in } m\}$

Causally computable means that variable x can be computed using equation m, assuming that the remaining variables in m are known. Then, Algorithm 7 in [12] computes the complete set of those subsets M' that guarantee the unknown variable computation. Hence, all these subsets M' have a causal complete matching. A *causal matching* is a matching such that all edges belong to $A_{\times}$. Thus a residual expression can be easily computed using a variable back substitution method, following the corresponding computation sequence. A *computation sequence* is a directed graph that shows how unknown variables can be substituted (or computed) in order to generate a residual. The computation sequence is directly derived from the complete matching.

2.3. Academic example

Next, an academic example based on an air compressor is described. The causal framework in [12] is applied to design a set of residuals which can be easily computed using the variable back substitution method. Assume that the compressor behavior is modeled by the following equations:

$$m_1 \quad : \quad v(t) = k_v \cdot \omega_c(t) + R \cdot i(t) + L\frac{d}{dt}i(t) \tag{5a}$$

$$m_2 \quad : \quad J\frac{d}{dt}\omega_c(t) = k_t \cdot i(t) - B \cdot \omega_c(t) - \tau(t) \tag{5b}$$

$$m_3 \quad : \quad W(t) = g(\omega_c(t), p_{in}(t), p_{out}(t), T_{in}(t)) \tag{5c}$$

$$m_4 \quad : \quad \eta(t) = \text{Lookup-Table}(W(t), p_{in}(t), p_{out}(t)) \tag{5d}$$

$$m_5 \quad : \quad \tau(t) = C_p\frac{T_{in}(t) \cdot W(t)}{\eta(t) \cdot \omega_c(t)}\left(\left(\frac{p_{out}(t)}{p_{in}(t)}^{\frac{\gamma-1}{\gamma}}\right) - 1\right) \tag{5e}$$

Table 1 describes all model variables and parameters. According to the previous definitions, the following sets of equations and variables are defined:

- $M = \{m_1, m_2, m_3, m_4, m_5\}$
- $V = \{v, \omega_c, i, \tau, W, p_{in}, p_{out}, T_{in}, \eta\}$

Function g in (5c) describes the behavior of the compressor box, whereas expression (5d) determines the compressor efficiency, $\eta(t)$, by means of a look-up table. Note that both expressions are non-invertible. Therefore, the variables in the right hand side of both expressions are not causally computable.

Assume that the set of variables can be partitioned into the set of known variables $Z = \{v, i, W, p_{in}, p_{out}, T_{in}\}$ and the set of unknown variables $X = \{\omega_c, \tau, \eta\}$. Table 2 shows the biadjacency matrix of the graph $G = (M, X; A)$ that just involves unknown variables. Now, the set of edges A contains causal and non-causal edges which are respectively represented by crosses and triangles in the biadjacency matrix.

Applying Algorithm 7 in [12], the following three M' subsets are obtained from the structural model in Table 2: $M'_1 = \{m_1, m_2, m_4, m_5\}$, $M'_2 = \{m_1, m_3\}$ and $M'_3 = \{m_2, m_3, m_4, m_5\}$. The set of residuals can be obtained by applying a variable back substitution method. For instance, given subset M'_1 the following causal matching can be obtained: $\{(m_1, \omega_c), (m_2, \tau), (m_4, \eta)\}$. Thus, equation m_5 can be used as a redundant equation and the consistency relation corresponding to residual r_1 can be obtained following the computation sequence in Figure 1.

A much simpler consistency relation is obtained from subset M_2'. The corresponding causal matching is $\{(m_1, \omega_c)\}$. Considering equation m_3 as the redundant equation, consistency relation (6) can be straightforwardly derived following the computation sequence in Figure 2.

$$\begin{aligned} &h(v(t), i(t), W(t), p_{in}(t), p_{out}(t), T_{in}(t)) \\ &\qquad = W(t) - g(v(t) - Ri(t) - L\frac{d}{dt}i(t), p_{in}(t), p_{out}(t), T_{in}(t)) = 0 \end{aligned} \tag{6}$$

Remark that this computation sequence satisfies the causal computability requirement. Therefore, a causally computable residual is directly derived from (6) as

$$r_2(t) = h(v(t), i(t), W(t), p_{in}(t), p_{out}(t), T_{in}(t)) \tag{7}$$

Following a similar procedure residual expression r_3 could be obtained for subset M_3'. The set of residuals r_1, r_2 and r_3 could be used to detect and isolate faults. For instance, assume a fault concerning the electrical resistance of the motor winding. This fault would imply the misbehavior of equation m_1 in (5a). Thus, this fault could be detected by residuals r_1 and r_2 since both subsets M_1' and M_2' include equation m_1.

Now, assume that measured variables were noisy. Therefore, the computation of variable $\omega_c(t)$ through m_1 and variable $\tau(t)$ through m_2 would not be desirable since it would imply the differentiation of noisy signals, leading to a bad performance. This means that $\omega_c(t)$ and $\tau(t)$ should be set as non-causally computable in m_1 and m_2 respectively. Thus Table 2 should

be replaced by Table 3. Then, under this new setting, Algorithm 7 in [12] would not produce any subset since the causal computability requirement could not be satisfied. For instance, remark that now M_2' is not feasible since there does not exist any causal matching involving equations m_1 and m_2. Thus, the fault concerning the electrical resistance of the motor winding would no longer be detectable.

In this present paper, residuals will be computed such that the computability of the unknown variables is ensured. In order to do so, causally computable sub-models M' will be first computed, then the corresponding computation sequences will be derived from each sub-model M' and finally the residuals will be evaluated to detect and isolate faults for the FCS system.

3. Fuel Cell Stack System

3.1. System description

The model used in this work is developed in [9]. The model is widely accepted in the control community as a good representation of the behavior of a FCS system. For the sake of space saving, the full model is not detailed here. The interested reader is referred to the aforementioned reference. The system model schema is depicted in Figure 3. The cathode side consists of an air compressor to feed atmospheric air to the cathode, the supply manifold that connects the compressor output with the air cooler input, and the air cooler and the static humidifier, that respectively refrigerates and humidifies the air before it goes into the stack. The model guarantees the required stoichiometry by regulating the hydrogen, supplied from a pressurized or liquid hydrogen tank, by means of a controlled valve. The electrochemical princi-

ples of the fuel cell stack are also modeled in order to accurately evaluate the electricity production and the outputs of the stack. This implies specific model equation for the anode, the cathode, the membrane and the stack voltage. Finally, the cathode outlet manifold of the fuel cell is considered in the model as an external component.

The model only describes the normal operational mode. Hence purges in the anode side are not considered. This means that all the hydrogen in the anode side is consumed. It is also assumed that the temperature of the fuel cell stack ($T_{st}(t)$) is known and constant since its dynamic behavior is much more slower than that of the rest of the model. These two assumptions reduce the complexity of the model by not considering discrete behaviors nor thermodynamic equations for the stack model. The resulting FCS system model is a complex and large-scale model involving 96 equations.

The available sensors in the system is another important issue to take into account for fault diagnosis. We assume that the following sensors installed in the system: the compressor motor speed ($\omega(t)$), the compressor output flow ($W_{cp}(t)$), the supply manifold output temperature ($T_{sm}(t)$) and pressure ($p_{sm}(t)$), the static humidifier temperature ($T_{sh}(t)$) and pressure ($p_{sh}(t)$), the outlet manifold flow ($W_{om}(t)$) and pressure ($p_{om}(t)$), and the cathode output pressure ($p_{ca}(t)$). In order to determine the set of sensors for fault diagnosis, several methodologies exist in the model-based diagnosis literature. Here, the optimal set of sensors has been chosen to ensure that convenient consistency relations can be finally designed [12]. The costs of sensors measuring pressures and temperatures are set to low values since such sensors are reliable, cheap and easy to install. On the other hand, humidity sensor costs

have high values since they are not desirable. Flow and speed sensors have intermediate cost values. As a result, the chosen sensors involve as much pressures and temperatures readings as possible.

Furthermore, there are other variables assumed to be known. This is the case of atmospheric variables such as humidity ($\phi_{atm}(t)$), temperature ($T_{atm}(t)$) and pressure ($p_{atm}(t)$). Similar assumption is done for the inlet anode hydrogen humidity ($\phi_{an,in}(t)$) since the hydrogen comes from a pressured tank where the humidity can be known. The desired air temperature ($T_{des}(t)$) and the desired air humidity (ϕ_{des}) are setpoints and therefore regarded as known variables. Also, the original model has an external controller which controls the compressor voltage ($v_{cp}(t)$) by means of the stack current ($i_{st}(t)$), consequently these two variables are also known due to control purposes.

3.2. Fault description

A set of seven faults has been defined in the FCS system. The faults are defined such that either a parameter or a variable is modified in only one specific model equation.

Faults f_{cp1}, f_{cp2}, f_{sm}, f_{st} and f_{om} are simulated as multiplicative faults where the corresponding parameters or variables are proportionally modified. On the other hand, faults f_{ac} and f_{sh} are simulated as additive faults, where an offset is added to their corresponding values. In order to introduce theses variations caused by faults, seven new parameters α_{f_i}, one for each fault, are introduced in the model. Next, the models for these faults are detailed.

3.2.1. Compressor faults

There are two compressor faults, f_{cp1} and f_{cp2}. Fault f_{cp1} represents an electric fault where the electrical resistance varies (e.g. due to an overheating). Specifically, it affects the electric resistance, R, in the following electric motor equation:

$$v_{cp}(t) = k_v \cdot \omega(t) + R \cdot i_{cp}(t) \tag{8}$$

where $v_{cp}(t)$ is the motor compressor voltage, k_v is the speed-to-voltage coefficient, $\omega(t)$ is the compressor angular speed and $i_{cp}(t)$ is the motor current. The presence of this fault is simulated by modifying the electric resistance, $R^{faulty} = \alpha_{f_{cp1}} \cdot R$ (for $0 \leq \alpha_{f_{cp1}} < 1$).

Fault f_{cp2} represents a malfunction of the compressor box. To characterize the relation among the compressor pressure, $p_{cp}(t)$, the motor speed, $\omega(t)$, and the normalized compressor flow rate $\Phi(t)$, the model uses a compressor map proposed in [13]. This compressor map involves non-linear equations, therefore it is condensed in a non-linear and non-invertible function:

$$\Phi(t) = \text{CompressorMap } (\omega(t), p_{cp}(t), T_{amb}(t)) \tag{9}$$

The corresponding fault is simulated by changing the computed flow, $\Phi^{fauty}(t) = \alpha_{f_{cp2}} \cdot \Phi(t)$ (for $0 \leq \alpha_{f_{cp2}} < 1$).

3.2.2. Supply manifold fault

The supply manifold is affected by fault f_{sm} which represents a leak or a partial blocked pipe. It is modeled by a loss of the output air flow, $W_{sm}(t)$, calculated in the next linearized equation of a nozzle model:

$$W_{sm}(t) = k_{sm}(p_{sm}(t) - p_{sm,ds}(t)) \tag{10}$$

where k_{sm} is the orifice constant, $p_{sm}(t)$ is the supply manifold pressure and $p_{sm,ds}(t)$ is the supply manifold downstream pressure. The presence of the fault implies that $W_{sm}^{faulty}(t) = \alpha_{f_{sm}} \cdot W_{sm}(t)$ (for $0 \leq \alpha_{f_{sm}} < 1$).

3.2.3. Air cooler fault

The air cooler fault, f_{ac}, represents a general malfunction of this device. As a consequence the air is not cooled to the desired temperature. This is simulated by setting an offset in the air cooler output air temperature:

$$T_{ac}^{faulty}(t) = T_{des}(t) + \alpha_{f_{ac}} \tag{11}$$

where $\alpha_{f_{ac}}$ is the temperature variation in Kelvins due to air cooler fault. Note that in this case the fault is additive, therefore the fault is present whenever $\alpha_{f_{ac}} \neq 0$.

3.2.4. Static humidifier fault

The static humidifier fault, f_{sh}, represent a malfunction in the humidifier device. Similar to the air cooler fault, the humidifier fault is simulated by an offset in the desired setpoint:

$$\phi_{sh}^{faulty}(t) = \phi_{des}(t) + \alpha_{f_{sh}} \tag{12}$$

Here the fault is also additive and $\alpha_{f_{sh}}$ indicates the excess or lack of relative humidity in the air caused by a fault in the humidifier device.

3.2.5. Fuel cell stack fault

Next fault, f_{st}, affects the fuel cell stack. It represents a failure in the outlet cathode (e.g. the outlet is partially stuck). Specially, it affects the

cathode outlet air flow $W_{ca}(t)$ calculated from:

$$W_{ca}(t) = k_{ca}(p_{ca}(t) - p_{st,ds}(t)) \tag{13}$$

where k_{ca} is the flow resistance constant, $p_{ca}(t)$ the cathode pressure and $p_{st,ds}(t)$ the stack downstream pressure. The fault is simulated by $W_{ca}^{faulty}(t) = \alpha_{f_{st}} \cdot W_{ca}(t)$ (for $0 \leq \alpha_{f_{st}} < 1$).

3.2.6. Outlet manifold fault

Last fault f_{om} affects the outlet manifold, that is characterized by means of a non-linear nozzle:

$$W_{om}(t) = \text{NonlinearNozzle } (p_{om}(t), p_{om,ds}(t), T_{om}(t)) \tag{14}$$

where $W_{om}(t)$ is the output flow, the $p_{om}(t)$ is the manifold pressure and the $T_{om}(t)$ is the inlet air temperature. The fault f_{om} is simulated by a change of the $W_{om}(t)$, i.e. $W_{om}^{faulty}(t) = \alpha_{f_{om}} W_{om}(t)$ (for $0 \leq \alpha_{f_{om}} < 1$), and it represents either a leak or an outlet obstruction.

Table 4 summarizes the set of proposed faults as well as their corresponding affected model variable or parameter. Note that other faults could be easily included in this set by modifying other variables or parameters in some model equations.

4. Consistency relations design for the FCS system

In this section, the different sets of model equations selected to construct a reduced set of consistency relations are presented in order to generate the desired residuals. But first, the steps to obtain these consistency relations are briefly detailed.

1. A structural model of the whole system is constructed. This model involves 96 equations and takes into account the causal computability of the unknown variables.
2. A set of 63 sub-models M' are derived applying Algorithm 7 in [12] to the structural model. With this sub-models, it is possible to detect and fully isolate all the preestablished faults.
3. A reduced set of sub-models M' such that all faults are detectable and fully isolable is sought. The selection criterion is fault isolability maximization so sub-models that are each sensible to a large number of faults are penalized. This problem can be easily solved applying Binary Integer Linear Programming techniques [14]. Finally, seven out of the 63 sub-models are selected, each one sensitive to only one single fault.

For each selected sub-model, it is possible to construct a consistency relation involving one fault and therefore derive from it a residual sensitive to that fault. This will facilitate the task of isolating faults since the fault signature involves a one-to-one correspondence between a residual and a fault.

Next, the seven sub-models are presented as well as the construction of the consistency relation. For the sake of clarity, the variables assumed to be known (see Section 3) will be signaled by an asterisk. Hence, these variables do not need to be computed from other model equations.

4.1. Sub-models for consistency checking

4.1.1. Sub-model for fault f_{cp1}

The first consistency relation is sensitive to the motor compressor fault f_{cp1}. It is constructed from the dynamic motor equation (15) used to de-

termine the motor speed from the motor torque $\tau_m(t)$ and the compressor torque $\tau_{cp}(t)$.

$$\omega^*(t) = \frac{1}{J}\int_0^T (\tau_m(t) - \tau_{cp}(t))\,\mathrm{d}t \tag{15}$$

Both torque variables must be computed since their values are unknown. In (16) the motor torque is determined from the motor current $i_{cp}(t)$, the torque constant k_t, the friction torque coefficient B and the motor speed $\omega^*(t)$. Note that the motor current is determined from (17) which is the equation used to introduce fault f_{cp1} (see (8)). Thus, the consistency relation will be sensitive to fault f_{cp1}.

$$\tau_m(t) = k_t \cdot i_{cp}(t) - B \cdot \omega^*(t) \tag{16}$$

$$i_{cp}(t) = \frac{1}{R}(v^*_{cp}(t) - k_v \cdot \omega^*(t)) \tag{17}$$

On the other hand, the compressor torque is determined from the thermodynamic equation (18) where C_p is the specific heat capacity of air, γ is the ratio of the specific heat of air, $\eta(t)$ is the compressor efficiency which is computed from (20), $p_{ratio}(t)$ is the ratio between output and input pressure determined from (19), and finally $W_{cp}(t)$ is the measured compressor flow.

$$\tau_{cp}(t) = C_p \frac{T^*_{atm}(t)}{\eta}(p_{ratio}(t)^{\frac{\gamma-1}{\gamma}} - 1)W^*_{cp}(t) \tag{18}$$

$$p_{ratio}(t) = \begin{cases} 0 & \text{if } p^*_{cp}(t)/p^*_{atm}(t) \leq 0 \\ p^*_{cp}(t)/p^*_{atm}(t) & \text{if } 0 < p^*_{cp}(t)/p^*_{atm}(t) < 1000 \\ 1000 & \text{if } p^*_{cp}(t)/p^*_{atm}(t) \geq 1000 \end{cases} \tag{19}$$

$$\eta(t) = \text{LookupTable}(W^*_{cp}(t), p_{ratio}(t)) \tag{20}$$

The output compressor pressure $p^*_{sm}(t)$ is assumed to be known since it is indeed the same as the supply manifold pressure, which is measured, then it holds that $p^*_{cp}(t) = p^*_{sm}(t)$.

It should be noted that the compressor efficiency $\eta(t)$ is determined by means of a look-up table, and the pressure ratio is bounded between 0 and 1000 bar by the saturation function (19). This implies that both equations, (19) and (20), are non invertible and thus it is not possible to compute, for example, p_{ratio} from (20). This fact was taken into account in the generation of the consistency relations.

4.1.2. Sub-model for f_{cp2}

The consistency relation sensitive to fault f_{cp2} is constructed as follows. First, the output compressor flow $W_{cp}^{*}(t)$ can be obtained from (21) where parameters ρ_a and d_c stand for air density and compressor diameter output, respectively. The variables to be determined are the compressor flow rate, $\Phi(t)$, and the compressor blade tip speed, $U_c(t)$.

$$W_{cp}^{*}(t) = \frac{p_{atm}^{*}(t)}{\sqrt{T_{atm}^{*}(t)/288}} \Phi(t) \rho_a \frac{\pi}{4} d_c^2 U_c(t) \tag{21}$$

The compressor flow rate is determined by the compressor map (22) which becomes inconsistent with the fault f_{cp2}. As in the previous case, $p_{ratio}(t)$ is computed from (19).

$$\Phi(t) = \text{CompressorMap } (\omega^{*}(t), p_{ratio}(t), T_{amb}^{*}(t)) \tag{22}$$

The blade tip speed is directly obtained from (23).

$$U_c(t) = \frac{\pi}{60} d_c \frac{\omega^{*}(t)}{\sqrt{T_{atm}^{*}(t)/288}} \tag{23}$$

4.1.3. Sub-model for fault f_{sm}

The consistency relation to detect the fault f_{sm} is mainly constructed from supply manifold equations. The air temperature is expected to decrease in the supply manifold, i.e. $T_{sm}(t) < T_{cp}(t)\ \forall t > 0$. Therefore, the pressure dynamic equation (24) is used in the model, where R_a is the gas constant, V_{sm} is the manifold volume. The variables to be computed are the output supply manifold flow, $W_{sm}(t)$, the compressor and manifold air temperatures, $T_{cp}(t)$ and $T_{sm}(t)$ respectively.

$$p^*_{sm}(t) = \frac{\gamma R_a}{V_{sm}} \int_0^T (W^*_{cp}(t)T_{cp}(t) - W_{sm}(t)T_{sm}(t))\,\mathrm{d}t \tag{24}$$

The output manifold flow is determined from (25) which is the faulty equation for fault f_{sm} introduced in Section 3.2. Note that the downstream pressure of the manifold is the output cathode pressure, which is measured. Hence, $p^*_{sm,ds}(t) = p^*_{ca}(t)$ should be considered in the consistency relation design.

$$W_{sm}(t) = k_{sm}(p^*_{sm}(t) - p^*_{sm,ds}(t)) \tag{25}$$

The compressor air temperature is determined by (26) where $p_{ratio}(t)$ and $\eta(t)$ are determined from (19) and (20) respectively.

$$T_{cp}(t) = T^*_{atm}(t) - \frac{T^*_{atm}(t)}{\eta(t)}(p_{ratio}(t)^{\frac{\gamma-1}{\gamma}} - 1) \tag{26}$$

Finally, the supply manifold air temperature is obtained from the ideal gas law, see (27), where the mass conservation principle is used in flow balance

(28) to compute the manifold mass $m_{sm}(t)$.

$$T_{sm}(t) = \frac{V_{sm} p^*_{sm}(t)}{R_a m_{sm}(t)} \tag{27}$$

$$m_{sm}(t) = \int_0^T (W^*_{cp}(t) - W_{sm}(t))\,\mathrm{d}t \tag{28}$$

4.1.4. Sub-model for fault f_{ac}

This consistency relation is straightforwardly derived. Actually, due to the fact that the output air cooler temperature is measured, there is no need to use model information to detect fault f_{ac}. Equality (29) must hold as long as f_{ac} is not present.

$$T^*_{ac}(t) = T^*_{des}(t) \tag{29}$$

Note that, since no temperature change is considered in the static humidifier model, we assume that the temperature measurement $T^*_{sh}(t)$ is also valid for the air cooler device, i.e. $T^*_{ac}(t) = T^*_{sh}(t)$.

4.1.5. Sub-model for fault f_{sh}

The consistency relation for fault f_{sh} could be similarly derived as the f_{ac} case, if output humidity was measured. However, it is known that good humidity measurements are hard and expensive to obtain. Therefore, to exploit the model properties and at the same time make the approach more feasible, no humidity measurements were considered in the sensor selection. As a consequence, humidity changes are regarded in all devices from the compressor to the static humidifier. Specifically, relative humidity varies

from an initial humidity $\phi_1(t)$ to a final humidity $\phi_2(t)$, given two different pressures $p_1(t)$ and $p_2(t)$, and two different saturation pressures, $p_{sat}(T_1(t))$ and $p_{sat}(T_2 9t))$, according to:

$$\phi_{out}(t) = \frac{p^*_{out}(t) p_{sat}(T^*_{in}(t)) \phi_{in}(t)}{p^*_{in}(t) p_{sat}(T^*_{out}(t))} \tag{30}$$

The saturation pressure, $p_{sat}(T(t))$, depends on the air temperature $T(t)$ and is computed as [15]

$$\log_{10}(p_{sat}(T(t))) = a_4 T(t)^4 + a_3 T(t)^3 + a_2 T(t)^2 + a_1 T(t) + a_0 \tag{31}$$

where a_i ($i = \{0, 1, 2, 3, 4\}$) are piecewise coefficients that vary with the temperature[9, 16].

The gas mixture properties of the dry and vapor gas are also considered to construct this consistency relation. First, the output pressure is the sum of the dry and the vapor gas pressures (see (32)). Vapor pressure is determined in (33) from the saturation pressure of the humidifier $p_{sat}(T^*_{sh}(t))$ and the output air humidity $\phi_{sh}t)$ which, in the absence of fault, should be the desired humidity, $\phi^*_{des}(t)$ (see (34)).

$$p^*_{sh}(t) = p_{a,sh,out}(t) + p_{v,sh,out}(t) \tag{32}$$

$$p_{v,sh,out}(t) = \phi_{sh}(t) p_{sat}(T^*_{sh}(t)) \tag{33}$$

$$\phi_{sh}(t) = \phi^*_{des}(t) \tag{34}$$

On the other hand, dry gas pressure remains unaltered throughout the humidifier, i.e. $p_{a,sh,out}(t) = p_{a,sh,in}(t)$. Again, using the gas mixture property, $p_{a,sh,in}(t)$ is computed in (35), where $p^*_{ac}(t)$ is the measured outlet cooler

pressure and $p_{v,sh,in}$ is the inlet vapor air pressure. The later is determined from (36) where the cooler air humidity, ϕ_{ac} is needed.

$$p_{a,sh,in}(t) = p^*_{ac}(t) - p_{v,sh,in}(t) \tag{35}$$

$$p_{v,sh,in}(t) = \phi_{ac}(t) p_{sat}(T^*_{ac}(t)) \tag{36}$$

Since no humidity sensors is used, the cooler air humidity is related to the supply manifold air humidity, $\phi_{sm}(t)$, in (37) and this, in turn, is obtained from the compressor air humidity, $\phi_{cp}(t)$ in (38). The relative humidity contained in the output compressor air is obtained from atmospheric humidity ϕ_{atm} which is known.

$$\phi_{ac}(t) = \frac{p^*_{ac}(t) p_{sat}(T^*_{sm}(t)) \phi_{sm}(t)}{p^*_{sm}(t) p_{sat}(T^*_{ac}(t))} \tag{37}$$

$$\phi_{sm}(t) = \frac{p^*_{sm}(t) p_{sat}(T_{cp}(t)) \phi_{cp}(t)}{p^*_{cp}(t) p_{sat}(T^*_{sm}(t))} \tag{38}$$

$$\phi_{cp}(t) = \frac{p^*_{cp}(t) p_{sat}(T^*_{atm}(t)) \phi^*_{atm}(t)}{p^*_{atm}(t) p_{sat}(T_{cp}(t))} \tag{39}$$

The compressor air temperature $T_{cp}(t)$ is determined by means of expression (26). All the remaining variables involved in (37)-(39) are already known since, as mentioned before, it holds that $T^*_{ac}(t) = T^*_{sh}(t)$ and $p^*_{ac}(t) = p^*_{sm}(t) = p^*_{cp}(t)$.

4.1.6. Sub-model for fault f_{st}

To construct the consistency relation sensitive to fault f_{st}, we start with the computation of the outlet manifold pressure, $p_{om}(t)$, as in (40), where

V_{om} is the manifold volume. In this equation all variables, except output cathode flow $W_{ca}(t)$, are known. Therefore, the output cathode flow is determined from the outlet cathode model equation (41), which is the inconsistent equation in case of fault f_{st}.

$$p^*_{om}(t) = \frac{R_a}{V_{om}} \int_0^T T^*_{st}(t)(W_{ca}(t) - W^*_{om}(t))\,\mathrm{d}t \tag{40}$$

$$W_{ca}(t) = k_{ca,out}(p^*_{ca}(t) - p^*_{st,ds}(t)) \tag{41}$$

The stack downstream pressure $p^*_{st,ds}(t)$ is indeed the outlet manifold pressure $p^*_{om}(t)$, i.e. $p^*_{st,ds}(t) = p^*_{om}(t)$.

4.1.7. Sub-model for fault f_{om}

The last consistency relation is sensitive to f_{om} fault. This is directly obtained from the non-linear nozzle model (42) since all variables involved in are already known. According to Section 3.2, at the presence of fault f_{om}, the expression in (42) is not longer valid (it becomes inconsistent).

$$W^*_{om}(t) = \mathrm{NonlinearNozzle}(p^*_{om}(t), p^*_{om,ds}(t), T^*_{st}(t)) \tag{42}$$

Due to the fact that the exhausted air from the cathode is thrown to the atmosphere, the outlet downstream pressure is the same as the atmospheric pressure, i.e. $p^*_{om,ds}(t) = p^*_{atm}(t)$.

4.2. Residual computation for the fault diagnosis system

Now, deriving a consistency relation for each sub-model presented above is straightforward. In each sub-model, the first equation is used as a redundant equation and then its unknown variables are computed by backtracking

through the remaining equations, following the *computation sequence*. Figure 4 shows the computation sequence for each consistency relation.

After computing the unknown variables as depicted in Figure 4, every residual only depends on known variables and can therefore be expressed as in Equation (2). For this particular case, seven residuals are obtained, each one depending on the following known variables:

$$
\begin{aligned}
r_1(t) &= h_1(v_{cp}(t), \omega(t), W_{cp}(t), p_{sm}(t), p_{atm}(t), T_{atm}(t)) \\
r_2(t) &= h_2(\omega(t), W_{cp}(t), p_{sm}(t), p_{ca}(t), p_{atm}(t), T_{atm}(t)) \\
r_3(t) &= h_3(W_{cp}(t), p_{sm}(t), p_{ca}(t), p_{atm}(t)) \\
r_4(t) &= h_4(T_{sh}(t), T_{des}(t)) \\
r_5(t) &= h_5(W_{cp}(t), p_{sm}(t), T_{sm}(t), p_{sh}(t), T_{sh}(t), \phi_{des}(t), p_{atm}(t), T_{atm}(t), \phi_{atm}(t)) \\
r_6(t) &= h_6(p_{ca}(t), W_{om}(t), p_{om}(t), T_{st}(t)) \\
r_7(t) &= h_7(W_{om}(t), p_{om}(t), T_{st}(t), p_{atm}(t))
\end{aligned}
$$

5. Simulation results

The model of the FCS system presented in this work is available in Simulink [9]. In this section, previously designed residual generators are also implemented in Simulink in order to proof their diagnostic performance by means of several simulation runs.

Four kinds of sensors are considered: air flow sensors, angular speed sensors, pressure sensors and temperature sensors. To set up a more realistic scenario, white noise with a Gaussian distribution is added in the measure-

ments. Table 5 shows the nominal order of magnitude corresponding to every kind of sensor and its standard deviation.

In a more realistic approach, model uncertainties should be included. This is handled by modifying some nominal parameter values involved in the equations of the consistency relations. Hence, discrepancies between the FCS system model and the equations in the residual generators are obtained, which is always true for real applications. Table 6 shows the set of parameters that have been modified to simulate modeling errors. The different values considered in the FCS system model and in the residual generator equations are also detailed. Uncertainty in parameters not appearing in the residual generators is not taken into account since it would have no effect on the residual performance.

Figures 5- 7 show the residual responses obtained from a series of simulations. Specifically, Figure 5 depicts the residual responses when there is no fault in the system. Basic thresholds are set up from these responses and each residual is normalized so that its corresponding threshold is ± 1 for all plots (residual units are irrelevant). It is important to point out that in the absence of faults, residuals differ from zero due to the presence of noise and modeling errors (this can be specially noted for residual r_1 in plot (a)). In Figure 6, the residual responses under a compressor fault f_{cp1} are shown. Remark that the only residual that is activated is r_1, which is indeed the only residual sensitive to fault f_{cp1}. The remaining residuals behave as in the fault-free scenario in Figure 5. Note that this sensitivity/insensitivity property of the residuals was gained by a convenient choice of equations when the structural sub-models were derived. The remaining six faults were also

simulated and the corresponding activated residuals are shown in Figure 7. The remaining residual responses would correspond to the fault free case.

In all these simulations, fault magnitudes concerning multiplicative faults are quantified as follows: $\alpha_{f_{cp1}} = 0.99$, $\alpha_{f_{cp2}} = 0.95$, $\alpha_{f_{sm}} = 0.98$, $\alpha_{f_{st}} = 0.95$ and $\alpha_{f_{om}} = 0.98$. Concerning additive faults, the air cooler fault f_{ac} is simulated as an increment of $\alpha_{f_{ac}} = 0.4K$ in the desired air temperature, whereas the static humidifier fault f_{sh} is simulated as a $\alpha_{f_{sh}} = 1\%$ increment in the desired relative humidity of the air. Larger fault magnitudes would not present any problem since the affected residuals would become larger as well. However, smaller fault magnitudes may not activate the residual which would imply that the fault is not detected. Hence, more advanced techniques for residual evaluation would be required, such as signal filtering and conditioning, statistical properties evaluation, adaptive thresholds, etc. This part has intentionally been omitted in this work since the goal is to show that diagnosing FCS systems in particular, and complex systems in general, is possible by means of the right choice of suitable sub-models based on structural properties.

6. Conclusions

This paper focuses on the design of residual generators for an FCS system. Each designed residual is obtained from a specific and suitable set of non-linear model equations. Based on structural model properties, the methodology analyzes how the non-linear model equations can be combined in order to obtain the set of consistency relations required by the diagnosis system. This analysis is not trivial when dealing with non-linear equations

since causal computability must be enforced. However, the chosen framework for fault diagnosis system design, easily takes causalities into account.

The design methodology has been proved to be efficient when dealing with a model that involves a high number of equations and unknown variables. In this paper, the algorithm presented in [12] is used to automatically derive the structural sub-models. These sub-models offer suitable properties to easily obtain residuals, (i.e. different fault sensitivities and unknown variables computation). Thus, because of these properties, it should not be difficult to generate residuals automatically by combining the right equations according to the sub-models and then simulating them by means of standard simulators. However, in this paper, the software to automatically generate residual has not been implemented and residual equations have been manually rearranged instead.

The residual generators design methodology has been thoroughly described for an FCS system. Finally, some fault scenarios have been simulated, validating a good performance of the residuals. Note that, despite the noise and modeling errors, it is possible to determine the presence of a fault just by checking if the residual crosses the threshold. Furthermore, since each residual is only sensitive to a specific fault, it is straightforward to determine which of the possible faults has occurred. This shows that the developed residuals are a good starting point for a diagnosis system where certainly more advanced techniques can be applied on the proposed residuals in order to improve fault detection and isolation.

Future work could entail the design of a fault diagnosis system for a real PEM fuel cell stack station. This would require the parameter estimation of

the equations involved in the designed consistency relations.

7. Acknowledgments

This work has been funded by the Spanish Ministry of Science and Technology through project CICYT SHERECS DPI2011- 26243, by the European Commission through contract i-Sense FP7-ICT-2009-6- 270428, and supported by the Fonds National de la Recherche, Luxembourg, through project CO11/IS/1206050 (SeSaNet).

8. References

[1] J. Wu, X. Z. Yuan, H. Wang, M. Blanco, J. J. Martin, J. Zhang, Diagnostic tools in pem fuel cell research: Part i electrochemical techniques, International Journal of Hydrogen Energy 33 (2008) 1735 – 1746.

[2] F. Barbir, PEM Fuel Cells: Theory and Practice, Elsevier, 2005.

[3] L. A. M. Riascos, M. G. Simoes, P. E. Miyagi, On-line fault diagnostic system for proton exchange membrane fuel cells, Journal of Power Sources 175 (2008) 419 – 429.

[4] T. Escobet, D. Feroldi, S. de Lira, V. Puig, J. Quevedo, J. Riera, M. Serra, Model-based fault diagnosis in pem fuel cell systems, Journal of Power Sources 192 (2009) 216 – 223.

[5] A. Ingimundarson, A. G. Stefanopoulou, D. A. McKay, Model-based detection of hydrogen leaks in a fuel cell stack, Control Systems Technology, IEEE Transactions on 16 (2008) 1004 –1012.

[6] Q. Yang, A. Aitouche, B. Ould-Bouamama, Structural diagnosability of fuel cell stack system based on bond graph tool, in: Proceedings of IFAC Safeprocess'09, Barcelona, Spain.

[7] M. Blanke, M. Kinnaert, J. Lunze, M. Staroswiecki, Diagnosis and Fault-Tolerant Control, Springer, 2nd edition, 2006.

[8] J. Chen, R. Patton, Robust Model-Based Fault Diagnosis for Dynamic Systems, Kluwer Academic Publishers, Boston, 1999.

[9] J. T. Pukrushpan, A. Stefanopoulou, H. Peng, Control of Fuel Cell Power Systems Principles, Modeling, Analysis and Feedback Design, Springer, 2004.

[10] M. Krysander, J. Åslund, M. Nyberg, An efficient algorithm for finding minimal over-constrained sub-systems for model-based diagnosis, Systems, Man and Cybernetics, Part A: Systems and Humans, IEEE Transactions on 38 (2008).

[11] L. Travé-Massuyès, T. Escobet, X. Olive, Diagnosability analysis based on component supported analytical redundancy relations, Systems, Man and Cybernetics, Part A: Systems and Humans, IEEE Transactions on 36 (2006) 1146–1160.

[12] A. Rosich, E. Frisk, J. Aslund, R. Sarrate, F. Nejjari, Fault diagnosis based on causal computations, Systems, Man and Cybernetics, Part A: Systems and Humans, IEEE Transactions on 42 (2012) 371–381.

[13] P. Moraal, I. Kolmanovsky, Turbochanger modeling for automotive control applications, SAE Paper (1999).

[14] A. Rosich, R. Sarrate, F. Nejjari, Optimal sensor placement for FDI using binary integer linear programming, in: 20th International Workshop on Principles of Diagnosis (DX-09), Stockholm, Sweden, pp. 235 – 242.

[15] T. V. Nguyen, R. E. White, A water and heat management model for proton-exchange-membrane fuel cells, Journal of The Electrochemical Society 140 (1993) 2178–2186.

[16] R. E. Sonntag, C. Borgnakke, G. J. V. Wylen, Fundamentals of Thermodynamics, John Wiley & Sons Inc, 5th edition, 1998.

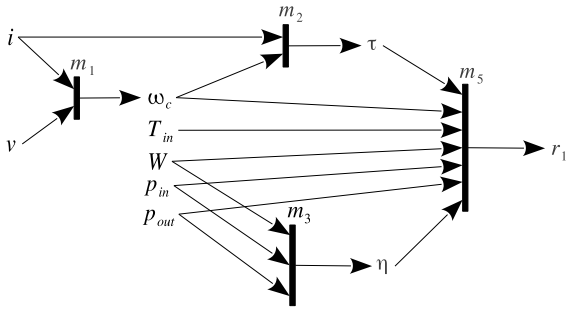

Figure 1: Computation sequence for subset M_1'.

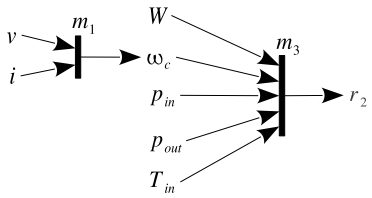

Figure 2: Computation sequence for consistency relation (6).

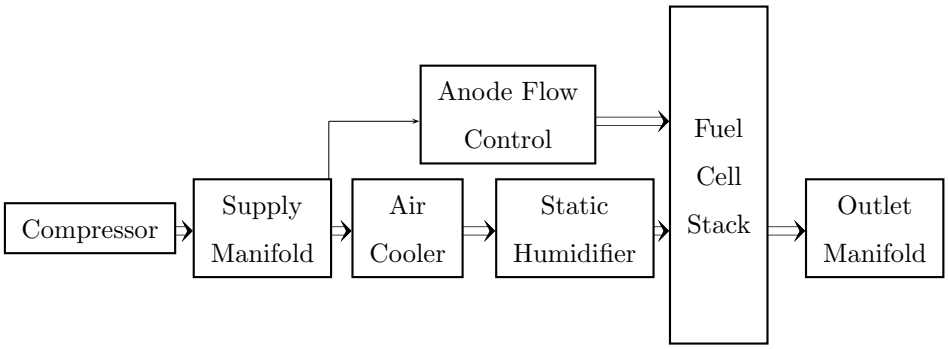

Figure 3: Fuel cell stack system.

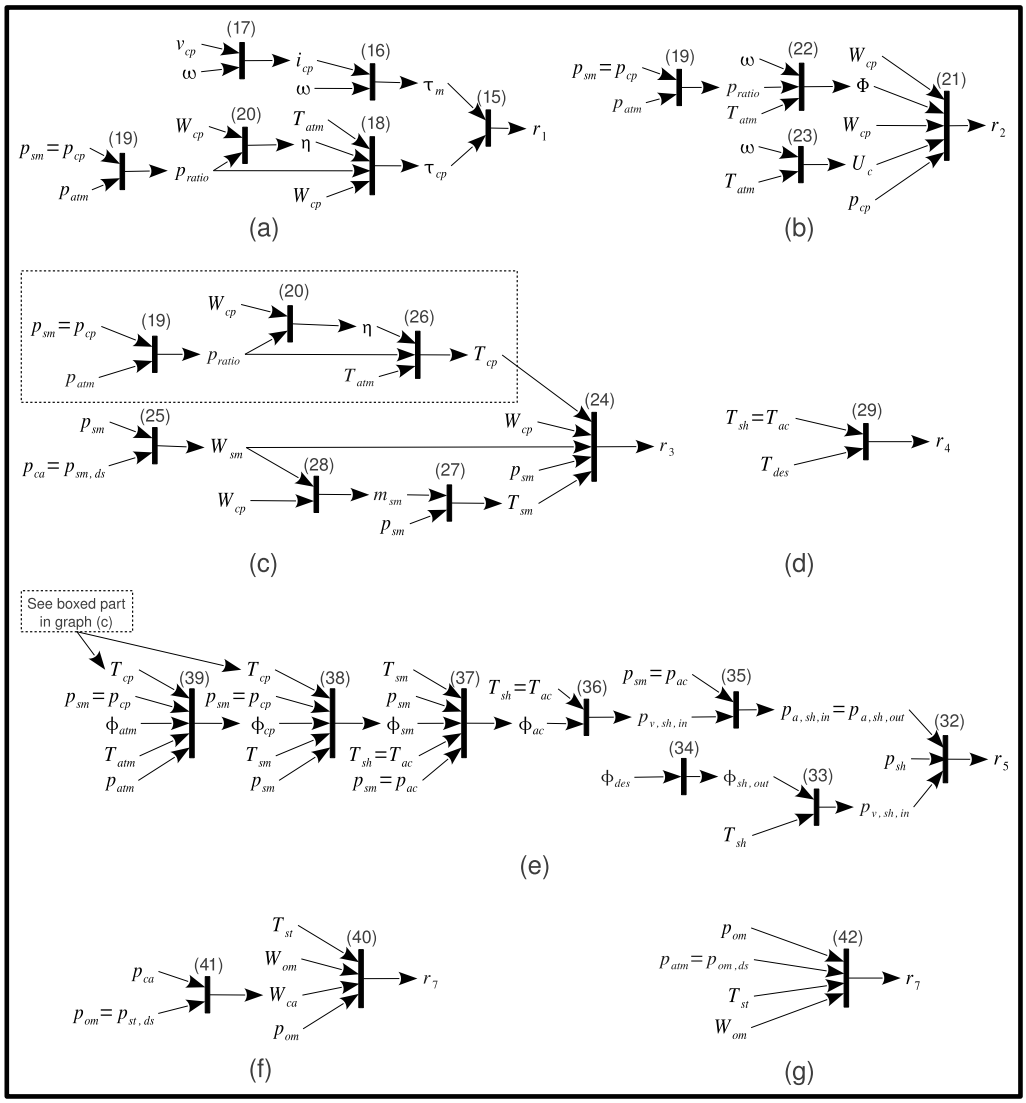

Figure 4: Residual computation sequences for: (a) f_{cp1}, (b) f_{cp2}, (c) f_{sm}, (d) f_{ac}, (e) f_{sh}, (f) f_{st}, (g) f_{om}.

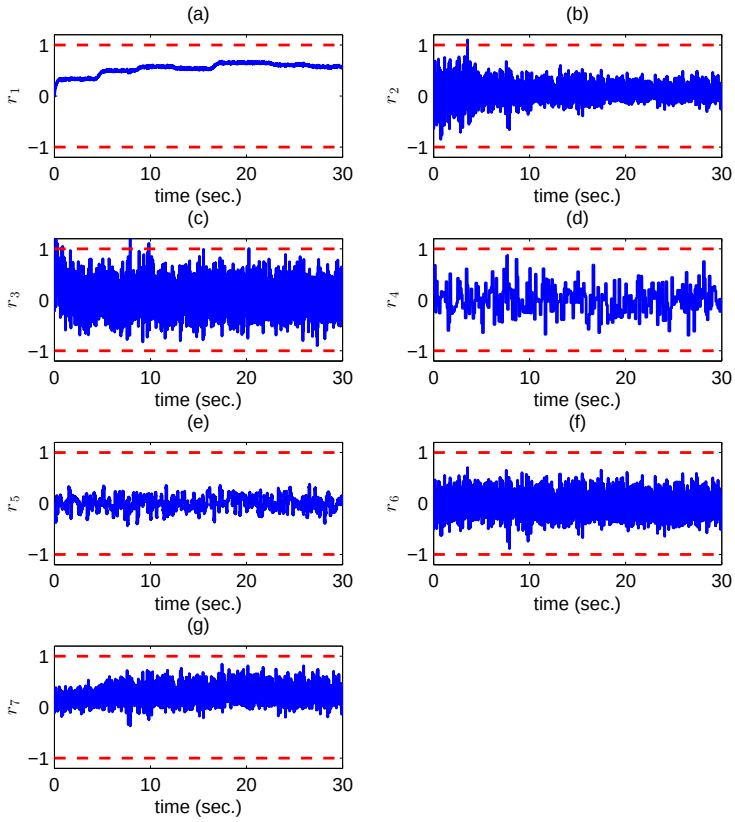

Figure 5: Residual responses for the free-fault scenario.

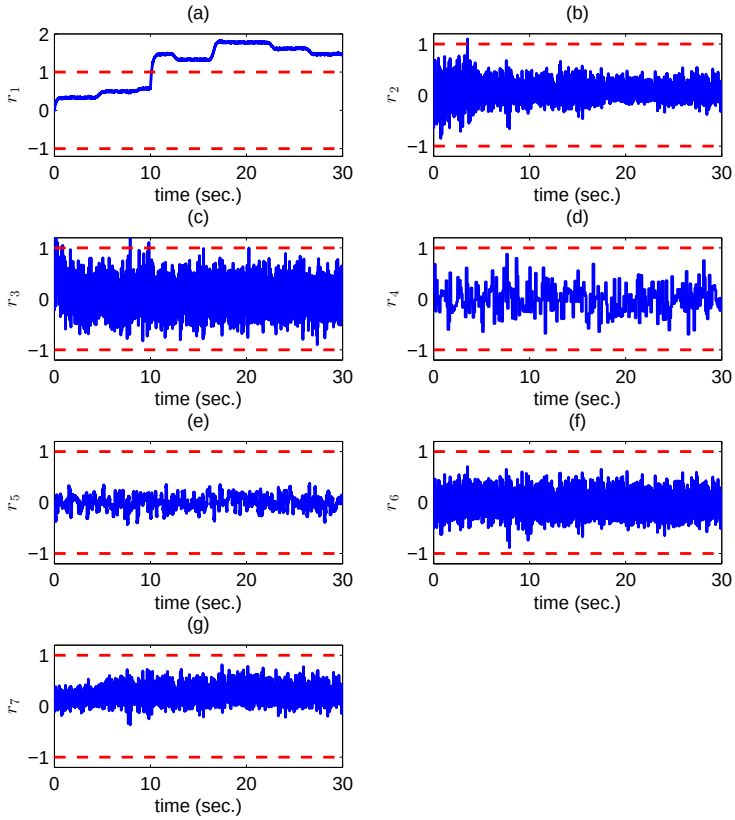

Figure 6: Residual responses for the compressor fault f_{cp1} scenario.

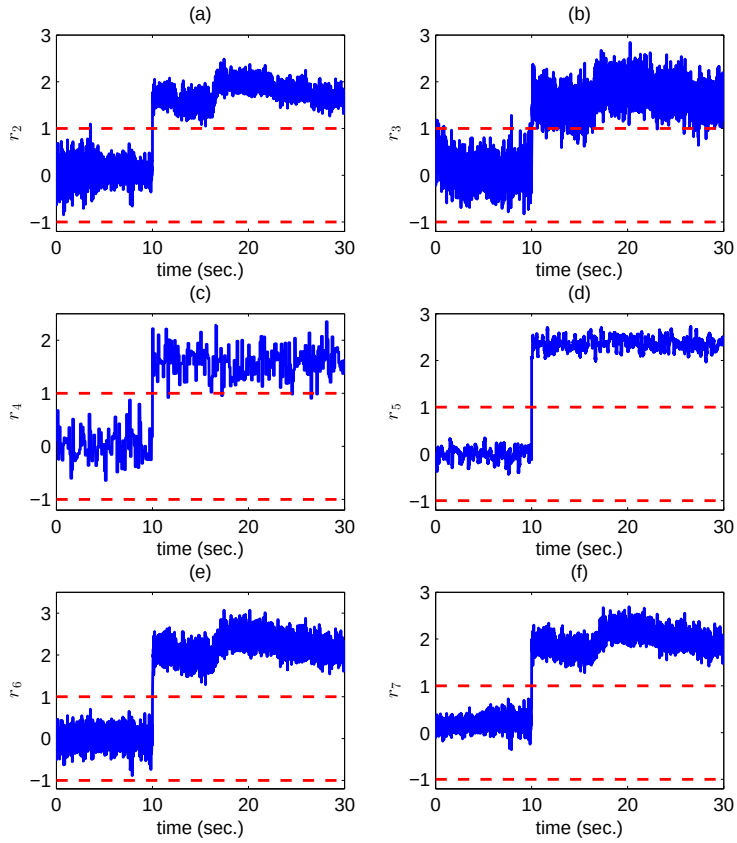

Figure 7: (a) Residual r_2 response for f_{cp2} fault. (b) Residual r_3 response for f_{sm} fault. (c) Residual r_4 response for f_{ac} fault. (d) Residual r_5 response for f_{sh} fault. (e) Residual r_6 response for f_{st} fault. (f) Residual r_7 response for f_{om} fault.

Variable	Description	Parameter	Description
$v(t)$	motor voltage	k_v	counter electromagnetic force
$\omega_c(t)$	angular speed	R	motor winding resistance
$i(t)$	motor current	L	motor inductance
$\tau(t)$	rotor torque	J	moment of inertia
$W(t)$	output air flow rate	k_t	torque coefficient
$p_{in}(t)$	input air pressure	B	viscous friction
$p_{out}(t)$	output air pressure	C_p	specific heat capacity of the air
$T_{in}(t)$	input air temperature	γ	specific heat ratio of the air
$\eta(t)$	efficiency		

Table 1: Air compressor variables and parameters.

	ω_c	τ	η
m_1	$\times$		
m_2	$\times$	$\times$	
m_3	Δ		
m_4			$\times$
m_5	$\times$	$\times$	$\times$

Table 2: Compressor structural model.

	ω_c	τ	η
m_1	Δ		
m_2	$\times$	Δ	
m_3	Δ		
m_4			$\times$
m_5	$\times$	$\times$	$\times$

Table 3: Compressor structural model with noisy measurements.

Fault	Affected variable or parameter	Fault description
f_{cp1}	R	compressor motor fault
f_{cp2}	$\Phi(t)$	compressor box fault
f_{sm}	$W_{sm}(t)$	supply manifold fault
f_{ac}	$T_{ac}(t)$	air cooler fault
f_{sh}	$\phi_{sh}(t)$	static humidifier fault
f_{st}	$W_{ca}(t)$	stack cathode fault
f_{om}	$W_{om}(t)$	outlet manifold fault

Table 4: FCS system faults.

	Nominal magnitude	Noise standard deviation
Air flow	$\backsim 0.1kg/s$	$4.5 \cdot 10^{-4}kg/s$
Angular speed	$\backsim 10^4 rad/s$	$10rad/s$
Air pressure	$\backsim 3 \cdot 10^5 Pa$	$300Pa$
Temperature	$\backsim 350K$	$0.07K$

Table 5: Noise standard deviation.

Parameter description	Symbol	In the FCS system simulator	In the residual generator	Units
Gas constant	R_a	289.9	287	$J/(kg \cdot K)$
Vapour molar mass	M_v	$18.015 \cdot 10^{-3}$	$18.02 \cdot 10^{-3}$	kg/mol
Compressor diameter outlet	d_c	0.2286	0.2287	m
Compressor inertia	J	$5.01 \cdot 10^{-5}$	$5 \cdot 10^{-5}$	kg/m^2
Speed-to-voltage coefficient	k_v	$15.3012 \cdot 10^{-3}$	$14.5 \cdot 10^{-3}$	$V/(rad/s)$
Current-to-torque coefficient	k_t	$22.496 \cdot 10^{-3}$	$24 \cdot 10^{-3}$	$N \cdot m/Amp$
Friction coefficient	B	$1.91 \cdot 10^{-5}$	$2 \cdot 10^{-5}$	$N \cdot m/(rad/s)$
Electric resistance	R	1.16	1.2	Ω
Supply manifold volume	V_{sm}	0.01838	0.02	m^2
Outlet manifold volume	V_{om}	$5.313 \cdot 10^{-3}$	$5 \cdot 10^{-3}$	m^2

Table 6: Modeling errors.